Open-Loop Response of a Burning Liquid Monopropellant

C. B. Allison* and G. M. Faeth†
Pennsylvania State University, University Park, Pa.

A direct comparison was obtained between the theoretical and experimental response of a burning liquid monopropellant surface to imposed pressure oscillations. The comparison extended beyond the quasi-steady frequency regime into the range where the combustion process interacts with the thermal wave in the liquid phase. The theory considered both gas and liquid-phase transient effects, involving a numerically integrated, first-order perturbation analysis. The experiment employed hydrazine as the test fuel, burning as a strand. With kinetic parameters fixed by steady burning rate measurements, the model gave good predictions of liquid-phase temperature distributions during steady combustion as well as the amplitude and phase of the oscillatory component of the burning rate in the presence of imposed pressure oscillations. The combustion response tends to peak in two frequency ranges; one corresponding to interaction with liquid-phase transient effects, which could be verified both theoretically and experimentally; the second corresponding to gas-phase transient effects, which could only be examined theoretically. Both ranges provide conditions where the amplifying power is sufficient to drive combustion instability.

Nomenclature

A = constant, Eq. (15)
a = vapor pressure parameter
B = pre-exponential parameter
C = constant, Eqs. (27) and (28)
C_f, C_p = specific heat of liquid and gas
D = diffusion coefficient
E = activation energy
h_i^0 = standard heat of formation of species i
L = heat of vaporization
L_f = vapor pressure parameter
M = molecular weight
n = reaction order
P = pressure
q = heat of combustion
R = gas constant
r = mass velocity
T = Temperature
t = time
u_i = burning rate constant, Eq. (38)
v = velocity
w = reaction rate
x = distance
$x_s, \dot{x}_s$ = position and velocity of surface
Y = mass fraction
β = specific heat ratio, Eq. (15)
γ = gas specific heat ratio
δ = temperature dependence of pre-exponential factor
δ_f = constant, Eq. (15)
ϵ = amplitude of pressure oscillation
η = dimensionless distance, Eq. (16)
θ = Shvab-Zeldovich variable, Eq. (17)
λ = thermal conductivity
ν_i, ν_i', ν_i'' = stoichiometry parameters, Eq. (8)
ρ = density
ϕ = phase angle
ω = frequency

Subscripts

f = liquid
F = fuel
s = surface
0 = steady-state quantities
1 = first-order quantities
∞ = far from liquid surface

Superscripts

$*$ = dimensional quantities

Received November 18, 1974; revision received March 24, 1975. This work was supported by NASA Grant NGR 39-009-077, under the technical management of R.J. Priem of the Lewis Research Center.

Index categories: Combustion in Heterogeneous Media; Combustion Stability, Ignition, and Detonation.

*Research Assistant, Department of Mechanical Engineering. Associate Member AIAA.

†Associate Professor of Mechanical Engineering. Member AIAA.

Introduction

Knowledge of the response characteristics of liquid combustion processes has received attention due to its importance with regard to combustion instability in liquid-propellant rocket engines. Past work in this area has involved a number of theoretical studies of bipropellant combustion response (see Ref. 1 and references cited therein). The objective of the present investigation was to consider the response of a liquid monopropellant, with emphasis on obtaining experimental results for comparison with theory.

The experimental apparatus involved the strand combustion of a liquid monopropellant, providing a one-dimensional geometry. Hydrazine was chosen as the test fuel, since its ability to burn with low velocity allows testing where the combustion process interacts with liquid-phase transient effects (a frequency regime where peak response is expected) while maintaining low test frequencies (1-10 Hz) for experimental accuracy.

The procedure of the investigation involved modeling the combustion process as a perturbation solution through first order in the amplitude of the pressure oscillation. The theory considers transient effects in both gas and liquid phases. Steady combustion measurements of burning rates and liquid temperature distributions were used to check the zero-order analysis. With satisfactory agreement at this point, comparison of theoretical and experimental oscillatory combustion results was then undertaken. The bounds of the

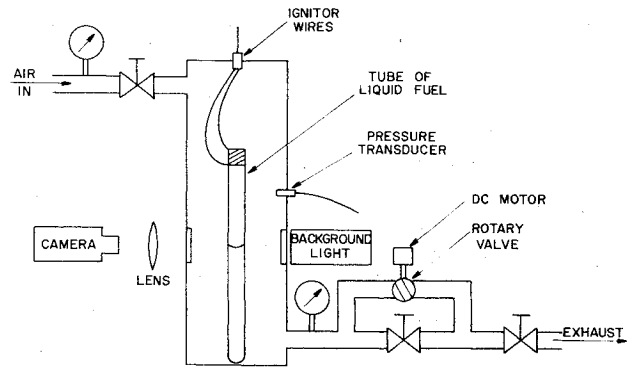

Fig. 1 Sketch of the oscillatory strand combustion apparatus.

linearized theory were determined by experimentally measuring the influence of the amplitude of the pressure oscillations on the combustion response. Using parameters that provided reasonable agreement between theoretical and experimental response characteristics, the implications of the results with regard to combustion instability characteristics were then examined.

Apparatus

A sketch of the strand combustion apparatus is shown in Fig. 1. A complete description of the system may be found in Ref. 2. The liquid hydrazine was contained in a glass tube and ignited at the top by means of a heater coil. Combustion caused the liquid surface to move down the tube, past the observation windows.

A rotary valve arrangement was used to provide oscillatory pressure variations within the test chamber.[3] This system allowed independent variation of the mean pressure, and the amplitude and frequency of the pressure oscillation in the test chamber.

The motion of the liquid surface was recorded as a shadowgraph on a 35 mm strip camera. The overall optical gain of the surface position measurements was 125:1. Chamber pressures were measured with a quartz transducer and recorded on an oscillograph. A synchronizing time signal was placed on both the strip camera and oscillograph records. Liquid-phase temperatures were measured in steady combustion tests, using a method described in Ref. 4.

Hydrazine (95 + % purity, obtained from Eastman Organic Chemicals Co.) was used for most tests. Analysis of this fuel indicated an actual composition of 98.6% hydrazine, 1.3% water, and 0.1% trace impurities. Testing was also done using 99.4% purity hydrazine (Matheson, Coleman, and Bell Corp.).

Theory

The present analysis of liquid monopropellant combustion is similar to solid-propellant combustion analysis of T'ien,[5] in many respects. A major distinction involves the observation of conventional phase equilibrium at the surface of the liquid,[4,6] and the use of this condition in the analysis, as opposed to the Arrhenius surface gasification rate of solid-propellant combustion.

The analysis considers both gas- and liquid-phase transient effects, and variable physical properties are treated in the gas phase. The combustion process is assumed to be one-dimensional, premixed, and laminar; with a one-step, irreversible reaction taking place. In the gas phase, the molecular weights and specific heats of all species are taken to be constant and equal; the gas is ideal; the Lewis number is unity; and the thermal conductivity is assumed to be independent of composition and proportional to temperature. In the liquid phase, properties are assumed to be constant, with negligible reaction and dissolved gas concentration.

Similar to earlier treatments,[5] the wavelength of the periodic pressure disturbance is assumed to be long in comparison with the width of the combustion process. Inertial and viscous effects are neglected, eliminating the need for considering the momentum equation.

The coordinate system is chosen to be fixed with respect to the mean position of the liquid surface, which has an instantaneous position $x_s^*(t^*)$. The chemical reaction is defined as follows; for N species in the system

$$\sum_{i=1}^{N} \nu_i' [i] - \sum_{i=1}^{N} \nu_i'' [i]$$

The equations of conservation of mass and energy in the liquid phase ($x^* < x_s^*(t^*)$) are

$$v_f^* = \text{constant} \tag{1}$$

$$(\partial T^*/\partial t^*) + v_f^* \partial T^*/\partial x^* = (\lambda^*/\rho^* C^*)_f \partial^2 T^*/\partial x^{*2} \tag{2}$$

The equations for conservation of mass, species, and energy in the gas phase [$x_s^*(t^*) < x^*$] are

$$(\partial \rho^*/\partial t^*) + \partial \rho^* v^*/\partial x^* = 0 \tag{3}$$

$$\rho^* (\partial Y_i/\partial t^*) + \rho^* v^* (\partial Y_i/\partial x^*) - (\partial/\partial x^*)$$

$$[\rho^* D^* \partial Y_i/\partial x^*] = \nu_i w_F^* \tag{4}$$

$$\rho^* C_p^* \frac{\partial T^*}{\partial t^*} + \rho^* v^* C_p^* \frac{\partial T^*}{\partial x^*}$$

$$- \frac{\partial}{\partial x^*} \left[\lambda^* \frac{\partial T^*}{\partial x^*} \right] - \frac{\partial P^*}{\partial t^*} = q^* w_F^* \tag{5}$$

where

$$w_F^* = B^* T^{*\delta} \left[\frac{P^{*Y} F}{M R^* T^*} \right]^n \exp \left[\frac{-E^*}{R^* T^*} \right] \tag{6}$$

$$q^* = - \sum_{i=1}^{N} \nu_i h_i^0 \tag{7}$$

$$\nu_i = \frac{(\nu_i'' - \nu_i')}{\nu_F'} \tag{8}$$

Since the liquid is incompressible, the cold-end boundary condition is

$$x^* \to -\infty \quad T^* \to T_{-\infty}^* \tag{9}$$

In addition to continuity of temperature and pressure at the liquid surface, there are four other conditions to be satisfied at this point. Conservation of mass at the moving surface reduces to

$$\rho_f^* (v_f^* - \dot{x}_s^*) = \rho^* (v^* - \dot{x}_s^*) \tag{10}$$

Conservation of energy yields

$$\lambda_f^* \left[\frac{\partial T^*}{\partial x^*} \right]_{s-} = \left[\lambda^* \frac{\partial T^*}{\partial x^*} \right]_{s+}$$

$$- \rho_f^* (v_f^* - \dot{x}_s^*) [(C_p^* - C_f^*) T_s^* + L^*] \tag{11}$$

The insolubility of the liquid phase to nonfuel gases provides

$$\left[\rho^* D \frac{\partial Y_F}{\partial x^*} \right]_{s+} = \rho_f^* (v_f^* - \dot{x}_s^*) (Y_{F,s} - 1) \tag{12}$$

Finally, the fuel mass fraction is related to the surface temperature through the Clausius-Clapeyron equation

$$Y_{F,s} = \frac{a^*}{P^*} \exp \left[\frac{-L_f^*}{R^* T_s^*} \right] \tag{13}$$

The remaining boundary conditions specify the fuel mass fraction and temperature in the gas phase far from the liquid surface. Since a gas-phase reaction of the form of Eq. (6) must eventually go to completion, this yields

$$x^* \to \infty \quad T^*(x^*,t^*) \to T^*_\infty(t^*) \quad Y_F \to 0 \tag{14}$$

where T^*_∞ is a known function of time, based upon the overall energy release of reaction and the form of the imposed pressure oscillations.

To simplify further developments, the following dimensionless quantities are defined:

$$\rho=\rho^*/\rho^*_{\infty 0} \quad T=T^*/T^*_{\infty 0} \quad v=v^*/v^*_{\infty 0} \quad P=P^*/P^*_0$$
$$\lambda=\lambda^*/\lambda^*_{\infty 0} \quad E=E^*/R^*T^*_{\infty 0} \tag{15a}$$

$$L_f=\frac{L^*_f}{R^*T^*_{\infty 0}} \quad L=\frac{L^*}{C^*_pT^*_{\infty 0}} \quad q=\frac{q^*}{C^*_pT^*_{\infty 0}}$$
$$\beta=C^*_f/C^*_p \quad \delta_f=\rho_f\lambda_f/\beta \tag{15b}$$

$$a=\frac{a^*}{p^*_0} \quad t=\frac{t^*\rho^*_{\infty 0}C^*_pv^{*2}_{\infty 0}}{\lambda^*_{\infty 0}} \quad x=\frac{x^*\rho^*_{\infty 0}C^*_pv^*_{\infty 0}}{\lambda^*_{\infty 0}}$$
$$A=\frac{B^*T^{*\delta}_{\infty 0}\lambda^*_{\infty 0}}{\rho^{*2}_{\infty 0}v^{*2}_{\infty 0}C^*_P}\left[\frac{P^*_0}{MR^*T^*_{\infty 0}}\right]^n \tag{15c}$$

where the subscript, $\infty 0$, refers to a zero-order (steady-state) quantity, evaluated at infinity.

The treatment of variable gas-phase properties is accomplished by defining the following transformation

$$\eta=\frac{C^*_pv^*_{\infty 0}}{\lambda^*_{\infty 0}}\int_{x^*_s(t^*)}^{x^*}\rho^*\,dx^* \tag{16a}$$

$$r=\rho v+\frac{\partial}{\partial t}\int_{x_S(t)}^{x}\rho\,dx \tag{16b}$$

A Shvab-Zeldovich variable is also introduced

$$\theta=qY_F+T \tag{17}$$

The assumed ideal gas equation of state and gas-phase thermal conductivity variation yield

$$\rho T=\rho\lambda=P \tag{18}$$

A perturbation analysis is used for the solution of this set of equations, assuming that the amplitudes of oscillation are small. Noting that pressure is only a function of time, and seeking oscillatory solutions implies

$$P(t) = 1+\epsilon e^{i\omega t} \tag{19a}$$
$$T(\eta,t) = T_0(\eta)+\epsilon T_1(\eta)e^{i\omega t} \tag{19b}$$
$$\theta(\eta,t) = \theta_0(\eta)+\epsilon\theta_1(\eta)e^{i\omega t} \tag{19c}$$
$$r(t) = r_0+\epsilon r_1e^{i\omega t} \tag{19d}$$
$$x_s(t) = 0+\epsilon x_{s1}e^{i\omega t} \tag{19e}$$

where ϵ is the amplitude of the pressure oscillation.

Substituting Eqs. (15), (16), and (19) into Eqs. (1) and (2) yields the following zero-order (steady) and first-order equations in the liquid phase

$$\delta_f(d^2T_0/d\eta^2)-dT_0/d\eta=0 \tag{20}$$
$$\delta_f(d^2T_1/d\eta^2)-(dT_1/d\eta)-i\omega T_1=r_1dT_0/d\eta \tag{21}$$

with the boundary conditions

$$\eta\to-\infty \quad T_0\to T_{-\infty} \quad T_1\to 0 \tag{22a}$$
$$\eta=0 \quad T_0=T_{0s} \quad T_1=T_{1s} \tag{22b}$$

The solution of Eqs. (20-23) is

$$T_0=T_{-\infty}+[T_{0s}-T_{-\infty}]\exp(\eta/\delta_f) \tag{23}$$

$$T_1=\{T_{1s}+\frac{r_1}{\delta_f i\omega}[T_{0s}-T_{-\infty}]\}\times\exp\left[\frac{1+(1+4i\omega\delta_f)^{1/2}}{2\delta_f}\eta\right]-\frac{r_1}{\delta_f i\omega}\times[T_{0s}-T_{-\infty}]\exp(\eta/\delta_f) \tag{24}$$

In the gas phase, the zero-order equations immediately yield $r_0=\theta_0=1$, for all values of η. The zero-order form of the energy equation is

$$(d^2T_0/d\eta^2)-(dT_0/d\eta)+q^{1-n}AT_0^{1+\delta-n}(1-T_0)^n\exp(-E/T_0)=0 \tag{25}$$

with the boundary conditions

$$\eta=0 \quad \left[\frac{dT_0}{d\eta}\right]_{\eta=0+}=q+T_{0s}-1 \tag{26a}$$
$$T_{0s}=1-aq\exp[-L_f/T_{0s}] \tag{26b}$$
$$\eta\to\infty \quad T_0\to 1 \tag{26c}$$

Equation (25) was solved numerically. The three boundary conditions of Eq. (26) permit a unique value of A to be found, yielding the mean burning rate. To complete the numerical integration in the half-infinite domain of the gas phase, the asymptotic expansion of Eq. (25) at large η was considered. The form of the expansion depends upon the reaction order[2] as follows:

$$n=1 \quad T_0=1-C\exp\{(1-[1+4A\exp(-E)]^{1/2})/2\eta\} \tag{27}$$
$$n=2 \quad T_0=1-[A/q\exp(-E)\eta-C]^{-1} \tag{28}$$

where C is an unknown constant. The solution involved selecting a value for A and C using either Eq. (27) or Eq. (28) to generate starting values for integration at large but finite η. Equations (26) then provided two boundary conditions for determining unique values for A and C by double interaction. With this method, the outer boundary condition of Eqs. (26) is only satisfied at infinity, as opposed to the point where numerical integration began.

The first-order perturbation equations in the gas phase are

$$\frac{d^2\theta_1}{d\eta^2}-\frac{d\theta_1}{d\eta}-i\omega\theta_1=-\left[\frac{\gamma-1}{\gamma}\right]i\omega T_0 \tag{29}$$

$$\frac{d^2T_1}{d\eta^2}-\frac{dT_1}{d\eta}+T_1\left\{qw_0\left[\left[\frac{1+\delta-n}{T_0}\right]-\frac{n}{1-T_0}+\frac{E}{T_0^2}\right]-i\omega\right\}+\frac{nqw_0}{1-T_0}\theta_1=r_1\frac{dT_0}{d\eta}-\frac{d^2T_0}{d\eta^2}-\left[\frac{\gamma-1}{\gamma}\right]i\omega T_0-(n-1)qw_0 \tag{30}$$

The first-order burning rate perturbation r_1 is a constant and w_0 is

$$w_0 = (A/q^n)\,T_0^{\,1+\delta-n}\,(1-T_0)^n \exp[-E/T_0] \tag{31}$$

The boundary conditions of Eqs. (29) and (30) at the liquid surface, $\eta = 0$, are:

$$\left[\frac{dT_1}{d\eta}\right]_{\eta=0+} = r_1\left\{\frac{\rho_f \lambda_f}{2\delta_f^2 i\omega}\,[T_{0s} - T_{-\infty}]\right.$$

$$[\sqrt{1+4i\omega\delta_f} - 1] + T_{0s}(1-\beta) + L\}$$

$$+ T_{1s}\left[1 - \beta + \frac{\rho_f \lambda_f}{2\delta_f}\,(1+\sqrt{1+4i\omega\delta_f})\right]$$

$$- \left[\frac{dT_0}{d\eta}\right]_{\eta=0+} \tag{32}$$

$$\left[\frac{d(\theta_1 - T_1)}{d\eta}\right]_{\eta=0+} = r_1[1 - T_{0s} - q]$$

$$+ \theta_{1s} - T_{1s} + \left[\frac{dT_0}{d\eta}\right]_{\eta=0+} \tag{33}$$

$$\theta_{1s} - T_{1s} = aq\,\frac{L_f T_{1s}}{T_{0s}^{\,2}} \exp\left[\frac{-L_f}{T_{0s}}\right] + T_{0s} - 1 \tag{34}$$

The remaining boundary conditions are determined by considering the behavior of Eqs. (29) and (30) for large η. This yields

$$\eta \to \infty \quad \theta_1(\eta) \to T_1(\eta) \to (\gamma - 1)/\gamma \tag{35}$$

which is the form for isentropic flow.

The first-order problem involves the solution of two linear, second-order differential equations, Eqs. (29) and (30), involving an unknown constant, r_1. The five boundary conditions, Eqs. (32-35), are sufficient to complete the solution. The solution employed asymptotic treatment of the outer boundary, similar to the method used for the zero-order solution. The details of the procedure may be found in Ref. 2.

The first-order burning rate perturbation can be related to the experimentally observed liquid surface oscillation as follows

$$x_{s1} = r_1/(\rho_f i\omega) \tag{36}$$

Since x_{s1} and r_1 are complex numbers, both amplitude and phase angle can be compared between theory and experiment.

As a baseline, the response was also computed for the case where both the liquid and gas phases were quasi-steady. If the following general form for the strand burning velocity is taken

$$v_f^* = u_0^* + u_1^* P^{*n} \tag{37}$$

the oscillatory motion of the liquid surface becomes

$$x_{s1}^*/\epsilon = -n u_1^* P_0^{*n}/(i\omega^*) \tag{38}$$

The physical properties of hydrazine used in the calculations are listed in Table 1.[2]

Steady Combustion

Burning Rate Results

There was little difference in the burning velocities of the 98.6 and 99.4% purity materials, therefore, the lower purity material was used in the bulk of the tests. Increasing tube inside diameter from 4-12 mm caused a reduction in the burning velocity that has been observed by others.[4,7] This was due to surface tension phenomena providing more surface area (per unit cross-sectional area) for the combustion process. A correction was applied for this effect by plotting the data for various tube sizes at each pressure and extrapolating to an infinitely large tube.[2]

Table 1 Properties used in the theoretical model

Property	Value
$T^*_{-\infty}$ (K)	298
$T^*_{\infty 0}$ (K)	1345
δ	0
q^*(cal/g)	1180
L^*(cal/g)	410
L_f^*(cal/g)	9750
$\ell n\, a^*$(atm)	12.601
γ	1.126
ρ_f^*(g/cm^3)	1.0
C_f^*(cal/g-K)	0.74
C_p^*(cal/g-K)	0.74
$\lambda^*_{\infty 0}$(cal/cm-sec-K)	4.2×10^{-4}
λ_f^*(cal/cm-sec-K)	9.3×10^{-4}

Figure 2 shows the present corrected hydrazine burning rates as a function of pressure. The hydrazine burning rate data of Antoine[7] (stated to be 100% pure hydrazine in a 12.7-mm tube) is also shown on the figure. Antoine's results were in good agreement with the present data in a 12-mm inside diameter tube, and are slightly above the data corrected for surface tension effects, as discussed earlier.

Theoretical burning rates were obtained by fitting the zero-order (steady) theory at a particular correlation condition for various reaction orders and activation energies. When reaction order, activation energy, and correlating pressure are chosen, solution of the zero-order equations provides a value for A. The measured burning rate at this pressure then yields B^* through Eq. (15) and the properties in Table 1. With B^* fixed, the value of A at any other pressure provides the burning rate at that pressure for comparison with the measurements. The results of these calculations are shown in Fig. 2. Table 2 summarizes the conditions of correlation, for first and second-order reactions, and the computed value of B^* as a function of reaction order and activation energy.

In agreement with earlier work,[7-9] the combustion process is first order at low pressures, shifting to second order at pressures greater than atmospheric pressure (in the global sense). The effect of activation energy on the correlation of burning rate is seen to be small in Fig. 2. Therefore, activation energy was investigated as a parameter in the oscillatory portion of the investigation.

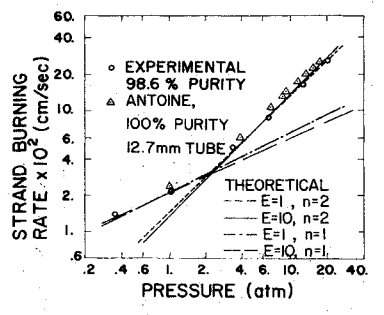

Fig. 2 Theoretical and experimental steady strand burning rates as a function of pressure.

Table 2 Global kinetic parameters used in the theoretical model[a]

E	E^* (Kcal/mole)	$B^*(n=1)$ (sec^{-1})	$B^*(n=2)$ (cm^3/g-sec)
1	2.673	3.473×10^4	7.608×10^7
10	26.73	7.468×10^9	8.385×10^{13}
15	40.08	...	3.749×10^{16}
30	80.16	...	8.446×10^{23}

[a] Correlation conditions: $n=1$; $P_0^*=1$ atm, $v_f^*=0.021$ cm/sec; and $n=2$; $P_0^*=6.7$ atm, $v_f^*=0.084$ cm/sec.

Liquid Temperature Results

Theoretical and experimental liquid-phase temperature distributions are compared at two different pressures in Fig. 3. The experimental temperature readings at positive distances result from the formation of a liquid film around the thermocouple as it leaves the surface, and should be disregarded.[4] The theoretical and experimental liquid-phase temperature distributions agree very well, providing confidence in the physical property values used in the analysis. Liquid-surface temperatures were also compared over the pressure range 0.5-20.4 atm, with good agreement between theory and experiment.[2] This provides justification for the assumption of conventional phase equilibrium at the liquid surface.

Oscillatory Combustion

Preliminary Measurements

With a reasonably satisfactory model of the steady hydrazine combustion process having been determined, oscillatory combustion was considered. Initial tests verified that oscillatory chamber pressure variations for a nonburning liquid column did not cause hydrodynamic disturbances that could be misinterpreted as a part of the combustion response.

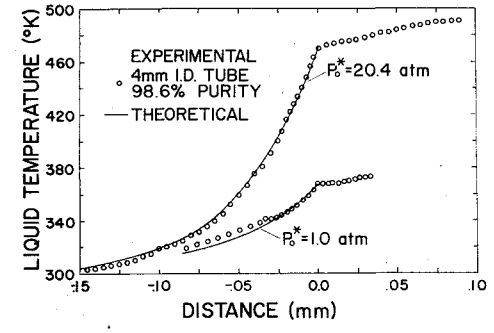

Fig. 3 Theoretical and experimental liquid phase temperature distributions.

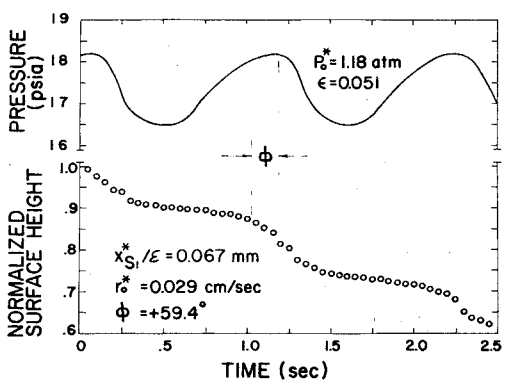

Fig. 4 Typical experimental pressure and liquid surface oscillations as a function of time.

Figure 4 shows a typical test record of pressure and liquid-surface position as a function of time for a combustion case. The results provide both the amplitude and phase angle (with respect to the pressure oscillations) of the liquid-surface oscillations. Repeatability between tests at the same condition gave maximum differences of 25%.

Pressure Oscillation Amplitude Effects

To determine the experimental bound of the linearized theory, a series of tests was conducted at a constant mean pressure and frequency, with varying pressure oscillation amplitude. The results of these tests are shown in Fig. 5, where both normalized surface oscillation amplitude x_{s_l}/ϵ and mean burning rate are plotted as a function of the normalized amplitude of the pressure oscillations ϵ.

In the linear regime, both x_{s_l}/ϵ and mean burning rate should be independent of ϵ. This linear regime is seen to extend to values of ϵ of about 0.20. At higher values of ϵ, both x_{s_l}/ϵ and the mean burning rate increase as a result of nonlinear effects. Based on these results, the remaining measurements were limited to $\epsilon<0.15$ to insure proper comparison with the linear model.

Response Measurements

Response measurements were made at mean pressures of 9.77 and 1.18 atm. Figures 6 and 7 show the amplitude and phase angle measurements at the higher pressure, along with theoretical results from both the quasi-steady theory, Eq. (38), and the unsteady theory for various activation energies.

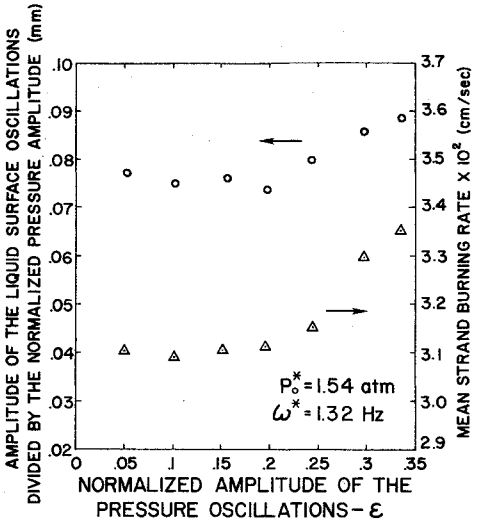

Fig. 5 Effect of pressure oscillation amplitude on liquid surface oscillation amplitude and mean burning rate.

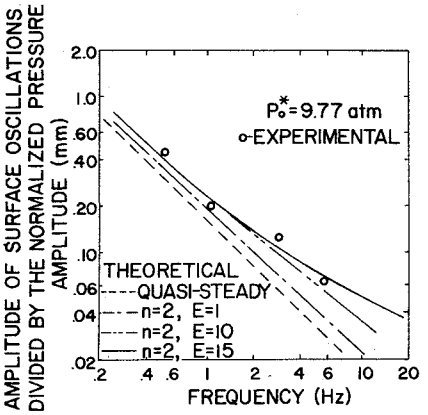

Fig. 6 Theoretical and experimental magnitude of the liquid surface oscillations as a function of frequency at a mean pressure of 9.77 atm.

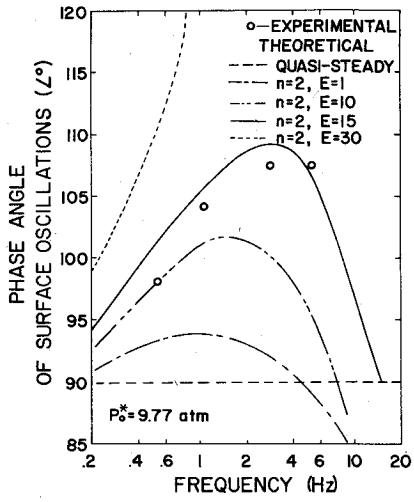

Fig. 7 Theoretical and experimental phase angle of the liquid surface oscillations as a function of frequency at a mean pressure of 9.77 atm.

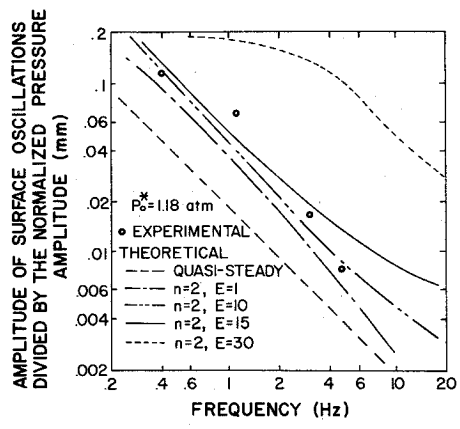

Fig. 8 Theoretical and experimental magnitude of the liquid surface oscillations as a function of frequency at a mean pressure of 1.18 atm.

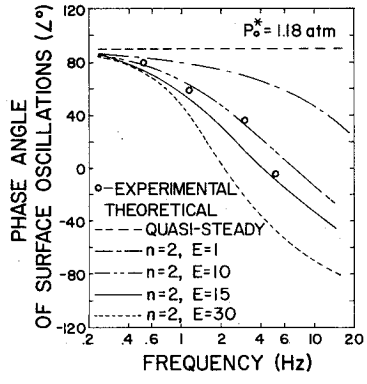

Fig. 9 Theoretical and experimental phase angle of the liquid surface oscillations as a function of frequency at a mean pressure of 1.18 atm.

While the unsteady theory allows for transient effects in both phases, it should be noted that the gas phase is essentially quasi-steady at these test conditions.

The assumed value of the activation energy in the transient theory has a greater influence on the oscillatory results than was the case for the prediction of mean burning rate. The results of Figs. 6 and 7 suggest a value of E in the range 10-15 for the best match between the transient theory and experiment with regard to both amplitude and phase angle.

The quasi-steady theory predicts a lower oscillation amplitude than the observed value, and always predicts that the burning rate is in phase with the pressure oscillation [which provides a constant 90° phase angle for the surface oscillation through Eq. (38)]. The results of Fig. 7 indicate a loss of quasi-steady behavior, with the burning rate oscillation leading the pressure oscillation. This is due to an interaction between the combustion process and liquid-phase transient effects. The interaction causes an increase in the combustion response, which can be seen by comparing the quasi-steady and transient predictions of the surface oscillation amplitude in Fig. 6.

Similar results at a pressure of 1.18 atm are illustrated in Figs. 8 and 9. As shown in Fig. 2, this pressure falls in the range where the mean burning rate is changing from first to second order. However, it was found that first-order kinetics in the transient theory could not provide a simultaneous match of both the amplitude and phase-angle data.[2] Therefore, second-order kinetics were considered. This involved recorrelation of the steady-state solution, since the original correlation (for second-order kinetics) shown in Fig. 2 yields too low a value for the steady burning rate at pressures near one atmosphere. The recorrelation only influences the value of B^*, which must be increased so that the mean burning rate agrees with the measured values. At each activation energy, the recorrelated values of B^* are 2.81 times larger than the values listed in Table 2 for a second-order reaction.[2] With this correction, values of E in the range 10-15 provided a good fit of both the amplitude and phase-angle data, as shown in Figs. 8 and 9. Notably, this activation energy range is the same as for the data at 9.77 atm.

The ratio of the quasi-steady to the actual amplitude of oscillation and the shift in phase angle from the 90° quasi-steady value is greater in Figs. 8 and 9 than at the higher pressure (Figs. 6 and 7). This occurs since the same experimental frequency range extends farther into the regime where transient liquid-phase effects are important (the characteristic frequency of the liquid phase has become smaller due to the lower burning rate at the lower pressure). At 1.18 atm, the burning rate lags the pressure oscillation, in contrast to the results at 9.77 atm where the burning rate was generally leading the pressure oscillation. The second-order transient theory is seen to model this lead-lag shifting of the burning rate properly.

Discussion

With the mean burning rate and liquid temperature distributions well matched by the zero-order theory, the first-order transient model provides a good estimation of the amplitude and frequency of the combustion response in the linear range. For hydrazine, the best estimation of the response was obtained with second-order global kinetics and E in the range 10-15 for pressures of 1.18 and 9.77 atm. The mean burning rate is shifting from first to second order at pressures near 1.18 atm. Therefore, the higher-order response characteristics dominate at mean pressures somewhat below the range where the mean burning rate shifts to higher order.

The previous results have concentrated on x_{sl} over the experimental range. Figure 10 illustrates the computed burning rate response characteristics over a wider range of conditions, with physical properties and kinetic parameters equivalent to hydrazine (more extensive results of this type may be found in Ref. 2). Two versions of the transient analysis are shown on the figure, the completely unsteady model discussed earlier and a version assuming a quasi-steady gas phase where transient phenomena are limited to the liquid phase.

From Fig. 10 one sees that, at lower frequencies the burning rate oscillation is in phase with the pressure oscillation, and both phases are quasi-steady. As the frequency approaches the characteristic frequency of the liquid-phase thermal wave, the phase and amplitude of r_l reached a peak in this region.[2]

As the frequency increases beyond the characteristic liquid-phase thermal wave frequency, gas-phase transient effects become important. Generally, the quasi-steady gas-phase

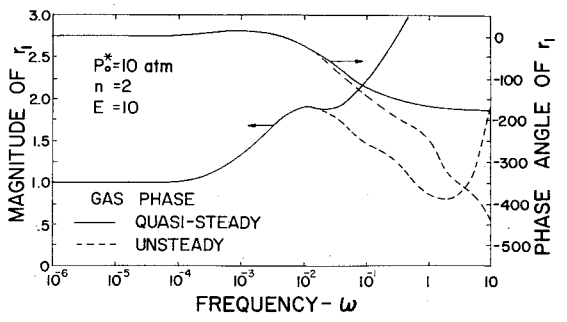

Fig. 10 Computed burning rate oscillation amplitude and phase angle as a function of frequency.

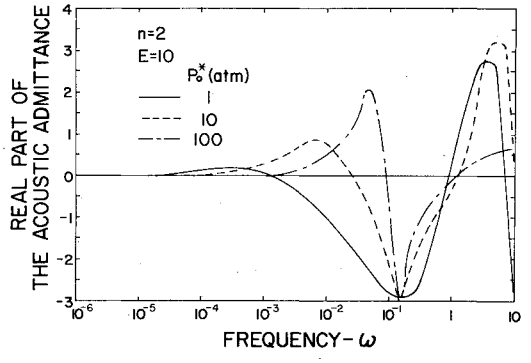

Fig. 11 Computed real part of the acoustic admittance as a function of frequency and pressure.

model no longer adequately represented the response for ω greater than $10^{-1} - 10^{-2}$. The gas-phase transient effects cause a reduction in the magnitude of r_f, reaching a minimum near the characteristic frequency of the gas phase, $\omega = 1$. A second peak response region is observed for dimensionless frequency values somewhat greater than unity. Higher frequencies cannot be considered by the present analysis, since inertial effects, etc., which have been neglected in the present analysis, become important. Despite the different boundary conditions at the surface, these general trends are similar to the computed results of T'ien[5] for homogeneous solid-propellant combustion response.

The real part of the acoustic admittance of the burning fuel is of interest in determining stability characteristics.[1] When gas-phase transient effects are important, this parameter varies with distance form the liquid surface, approaching a constant value at large distances. Using asymptotic analysis, the admittance was determined from the present calculations.[2] A portion of these results is shown in Fig. 11, for property values, etc. characteristic of hydrazine.

With increasing frequency, two positive peaks are observed in the real part of the acoustic admittance plotted in Fig. 1. The first peak occurs near the characteristic frequency of the liquid-phase thermal wave, while the second is associated with frequencies slightly above the gas-phase characteristic frequency. Between these two zones, damping associated with the onset of gas-phase transient effects results in negative admittance values. These general characteristics are also qualitatively similar to T'ien's[5] results for solid propellants.

Combustion instability is usually associated with values of the real part of the acoustic admittance greater than a value on the order of unity.[1] Table 3 summarizes the frequency ranges where this criterion is satisfied for the results of Fig. 11. The values have been converted to dimensional form, with the two frequency ranges corresponding to the liquid and gas-phase transient regimes. At atmospheric pressure, only the gas-phase transient range has sufficient amplification to drive instability, while at pressures greater than 10 atm, both regimes are of significance.

Table 3 Critical frequency ranges for strand combustion[a]

Mean pressure (atm)	Liquid transient range (Hz)	Gas transient range (Hz)
1	....	300-1500
10	15 (approx)	4500-21500
100	450-1650	>225,000

[a] Properties from Tables 1 and 2; $n = 2$, $E = 10$.

Combustion instability is usually associated with the frequency range 500-30,000 Hz.[1] At low pressures, Table 3 indicates that this range would involve gas-phase transient effects; while for pressures greater than 10 atm interaction of the combustion process with the liquid-phase thermal wave is the more significant phenomena. These findings suggest that, while the use of a quasi-steady gas-phase assumption at low pressures might be adequate for mean burning characteristics of monopropellants, potentially important contributions to the combustion response can be overlooked with this approach.

The relationship between the present results and the practical problem of droplet combustion in a liquid-fueled rocket engine is very approximate at best. Analysis of monopropellant droplet combustion indicates that strand and droplet behavior is similar when the reaction zone is close to the liquid surface.[10] This is the case for large droplets at elevated pressure. If this tentative relationship is accepted, the present study suggests that sufficient amplification is available to drive combustion instability for hydrazine within the frequency range usually associated with this phenomenon. The present results are only suggestive, however, more definitive results must await through consideration of droplet combustion response over the complete size range of droplets within a spray.

Conclusions

1) Measurements indicated that steady hydrazine strand combustion has a pressure dependence of ½ at subatmospheric pressures and unity at pressures above atmospheric. Conventional phase equilibrium at the liquid surface was observed throughout the range 0.5-20.4 atm.

2) For pressure oscillation amplitudes in the linear regime, at mean pressures of 1-10 atm, good predictions were obtained for the amplitude and phase angle of the liquid-surface oscillations using second-order global kinetics with E in the range 10-15. The observed shift from burning rate fluctuations lagging the pressure fluctuation at low pressures to leading them at high pressures was correctly modeled by the theory. The measurements indicated the onset of nonlinear effects for $\epsilon > 0.2$.

3) The combustion response of hydrazine peaks in two frequency ranges. The peak at lower frequencies was examined both theoretically and experimentally. It results from the interaction of the combustion process with the thermal wave in the liquid phase. The peak at higher frequencies was only examined theoretically. It corresponds to the interaction of the combustion process with gas-phase transient effects. This behavior is qualitatively similar to the response of homogeneous solid propellants, determined in Ref. 5 (which used a similar transient model).

4) Ranges of pressure and frequency were calculated where liquid hydrazine combustion exerts sufficient amplifying power to drive combustion instability, at frequencies corresponding to those usually associated with the phenomenon of combustion instability. At low pressures, this range was associated with gas-phase transient effects, while at high pressures the range corresponded to combustion interaction with the liquid-phase thermal wave. This suggests that gas-phase transient effects may be important to response characteristics at low pressures, where the gas phase might or-

dinarily be assumed to be quasi-steady. The application of these findings to droplet combustion is tentative at best, however, and the droplet case deserves further consideration.

References

[1]Harrje, D.T., ed, "Liquid-Propellant Rocket Combustion Instability," NASA SP-194, Washington, D.C., 1972, Chapt. 3.

[2]Allison, C.B., "Burning Rate Response of Liquid Monopropellants to Imposed Pressure Oscillations," NASA CR-134541, Jan. 1974; also Ph.D. thesis, March 1974, Pennsylvania State University, University Park, Pa.

[3]Chervinsky, A.P., Sirignano, W.A., Harrje, D.T., and Varma, A.K., "Axisymmetric Jet Diffusion Flame in an External Oscillating Stream," *Proceedings of the Sixth ICRPG Combustion Conference,* CPIA Publication 192, Applied Physics Lab., Johns Hopkins Univ., Baltimore, Md., Dec. 1969, pp. 171-180.

[4]Faeth, G.M., "High-Pressure Liquid Monopropellant Strand Combustion," *Combustion and Flame,* Vol. 18, Feb. 1972, pp. 103-113.

[5]T'ien, J.S., "Oscillatory Burning of Solid Propellants, including Gas-Phase Time Lab," *Combustion Science and Technology,* Vol. 5, May 1972, pp. 47-54.

[6]Faeth, G.M., "Prediction of Pure Monopropellant Droplet Life Histories," *AIAA Journal,* Vol. 8, July 1970, pp. 1308-1314.

[7]Antoine, A.C., "Mechanism of Burning of Liquid Hydrazine," *Proceeding of the Eighth Symposium (International) on Combustion,* Williams & Wilkins, Baltimore, Md., 1962, pp. 1057-1059.

[8]Gray, P. and Kay, J.C., "Stability of the Decomposition Flame of Liquid Hydrazine," *Research,* Vol. 8, Jan. 1955, pp. 53-55.

[9]Gray, P., Lee, J.C., Leach, H.A., and Taylor, D.C., "Propagation and Stability of the Decomposition Flame of Hydrazine," *Proceedings of the Sixth Symposium (International) on Combustion,* Reinhold, New York, 1956, pp. 255-263.

[10]Williams, F.A., *Combustion Theory,* first ed., Addison-Wesley, Reading, Mass., 1965, pp. 231-245.